ACS OMEGA

http://pubs.acs.org/journal/acsodf

Article

Argentatin C Analogues with Potential Antinociceptive Activity and Other Triterpenoid Constituents from the Aerial Parts of *Parthenium incanum*

Ya-ming Xu, E. M. Kithsiri Wijeratne, Aida Calderon-Rivera, Santiago Loya-López, Samantha Perez-Miller, Rajesh Khanna,* and A. A. Leslie Gunatilaka*

Cite This: *ACS Omega* 2023, 8, 20085−20095

Read Online

ACCESS | Metrics & More | Article Recommendations | Supporting Information

ABSTRACT: Four new triterpenes, 25-dehydroxy-25-methoxyargentatin C (**1**), 20*S*-hydroxyargentatin C (**2**), 20*S*-hydroxyisoargentatin C (**3**), and 24-*epi*-argentatin C (**4**), together with 10 known triterpenes (**5**−**14**) were isolated from the aerial parts of *Parthenium incanum*. The structures of **1**−**4** were elucidated by detailed analysis of their spectroscopic data, and the known compounds **5**−**14** were identified by comparison of their spectroscopic data with those reported. Since argentatin C (**11**) was found to exhibit antinociceptive activity by decreasing the excitability of rat and macaque dorsal root ganglia (DRG) neurons, **11** and its new analogues **1**−**4** were evaluated for their ability to decrease the excitability of rat DRG neurons. Of the argentatin C analogues tested, 25-dehydroxy-25-methoxyargentatin C (**1**) and 24-*epi*-argentatin C (**4**) decreased neuronal excitability in a manner comparable to **11**. Preliminary structure−activity relationships for the action potential-reducing effects of argentatin C (**11**) and its analogues **1**−**4**, and their predicted binding sites in pain-relevant voltage-gated sodium and calcium channels (VGSCs and VGCCs) in DRG neurons are presented.

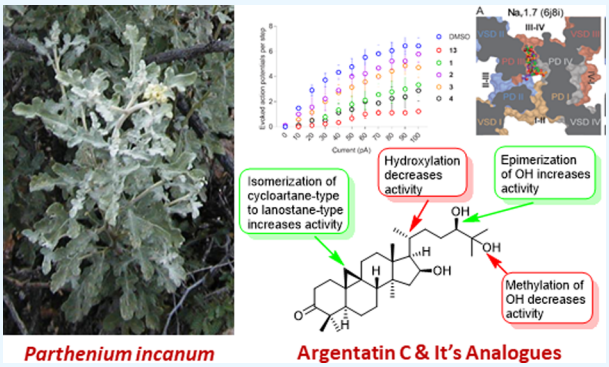

INTRODUCTION

Parthenium incanum Kunth (Asteraceae; common names: mariola, New Mexico rubber plant) is a deciduous shrub native to the Southwestern United States and the Chihuahuan desert of Northern Mexico.[1] Plants of the genus *Parthenium* find applications in Native American medicine to treat pain conditions.[2,3] For example, boiled fresh leaves of *P. incanum* are used by Jicarilla Apaches as a medicinal tea and to treat pregnancy-related discomfort by rubbing preparations over the abdomen.[2] Triterpenes including argentatin A, argentatin B, isoargentatin B, and incanilin have been reported from *P. incanum*.[4,5] Previous investigations have shown that argentatins A and B exhibit antimicrobial[6] and anti-inflammatory[7] properties, and cytotoxic activity against several cancer cell lines.[7−9] We have recently reported the occurrence of argentatins A−C and isoargentatin A in *P. incanum* and antinociceptive activity of argentatin C.[10]

Chronic pain is a pathological state characterized by hyperexcitable sensory neurons, leading to nociception in the absence of painful stimuli. Chronic pain affects about 20−30% of the world population.[11] Historically, humans have used natural remedies derived from plants for medicinal purposes to treat musculoskeletal, neuropathic, and inflammatory pain conditions. Notable examples of these plant-based antinociceptive agents include morphine (from opium poppy),[12] salicin (from willow bark),[13] tetrahydrocannabinol (THC from cannabis),[14] capsaicin (from chili peppers),[15] resiniferatoxin (RTX) from the cactus-like plant *Euphorbia resinifera* (Euphorbiaceae),[16] mitragynine from *Mitragyna speciosa* (kratom; Rubiaceae),[17] salvinorin A from *Salvia divinorum* (Mexican sage bush; Lamiaceae),[18] polygodial from *Drimys winteri* (Winteraceae),[19] and tetrahydropalmitine from *Corydalis yanhusuo* (Papaveraceae).[20] Of these, opioids are the cornerstone of management for many types of pain.[21,22] However, opioids are only partially effective in some pain types and patient populations including neuropathic pain and are often associated with serious side effects including tolerance, addiction, and death that limit their clinical utility.[23] Thus, there is an urgent need for new pain therapies (antinociceptive agents) to circumvent the liabilities of opioid drugs.

The International Association for the Study of Pain (IASP) defines pain as an unpleasant sensory and emotional

Received: April 10, 2023
Accepted: May 10, 2023
Published: May 25, 2023

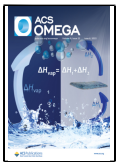

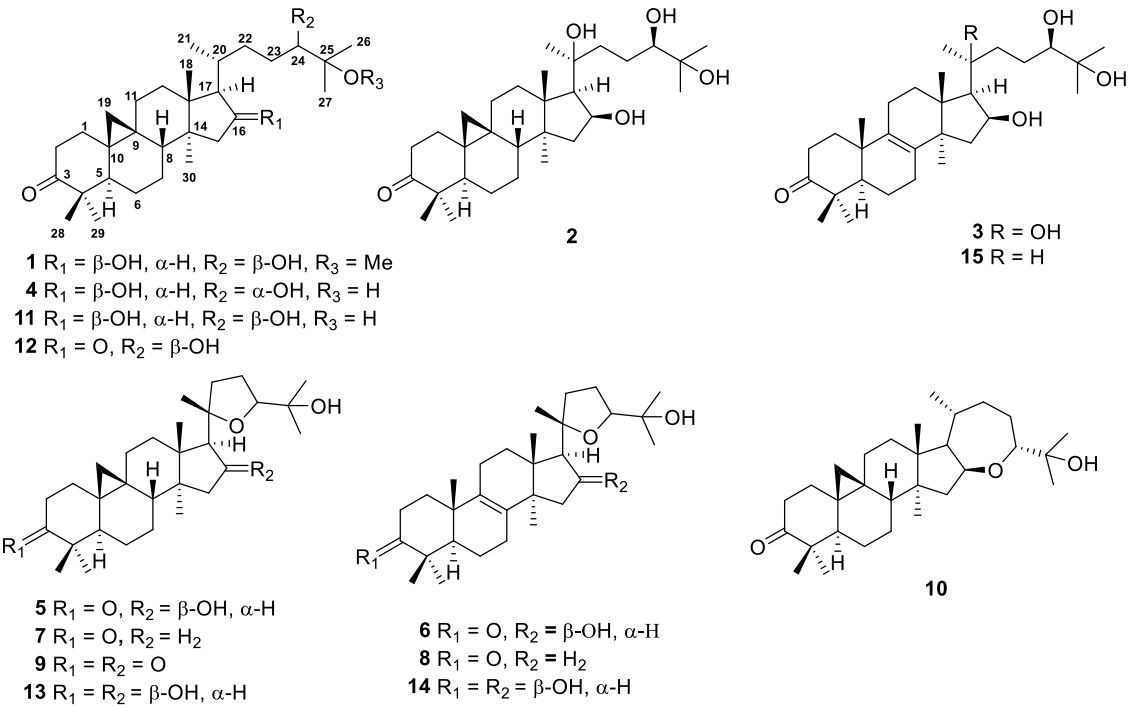

Figure 1. Structures of triterpenoids **1**−**14** from *P. incanum* and isoargentatin C (**15**).

experience associated with, or resembling that associated with, actual or potential tissue damage.[24] Nociceptors are a subgroup of sensory neurons specialized in the detection of painful stimuli.[25,26] The cell bodies of pain receptors are located in either the dorsal root ganglia (DRG) or the trigeminal ganglia (TG), connecting the peripheral nervous system with the central nervous system (CNS). The key physiological processes for the peripheral transmission of sensory information are transduction, action potential transmission, and transmitter release. In the periphery, the nerve endings have transmembrane proteins called ion channels and receptors, which transduce a noxious stimulus into an electrical signal. Among them, specific voltage-gated sodium channels (VGSCs) and voltage-gated calcium channels (VGCCs) contribute to reach the threshold for action potential generation and determine cellular excitability.[25,27] In addition, these channels support propagation of action potentials to the central terminals within the spinal cord.[28,29] Sustained noxious stimuli or chronic diseases may affect stimulus detection, action potential generation, and transmission, which facilitate nociceptive processing, resulting in transition from acute pain to chronic pathological pain conditions.[30] The hyper-activity of VGSCs and VGCCs in the peripheral tissue injury or in damaged nerve promotes it to become hyper-excitable.[28] Therefore, the discovery of molecules that modulate the excitability in DRG neurons is key to developing antinociceptive agents that target the activity of these ion channels in nociceptive neurons.[31]

Our search for natural products-based antinociceptive agents has thus far resulted in the identification of betulinic acid from *Hyptis emoryi*,[32] physalin F from *Physalis acutifolia*,[33] (−)-hardwickiic acid from *Croton californicus*,[34] hautriwaic acid from *Eremocarpus setigerus*,[34] and argentatin C (**11**) from *P. incanum*.[10] Encouraged by the ability of **11** to attenuate postoperative pain via inhibition of VGSCs and T-type VGCCs,[10] and the reported use of *Parthenium* species to treat pain conditions,[2,3] prompted us to undertake a detailed investigation of *P. incanum* for its antinociceptive constituents. Herein, we report the isolation and characterization of four new analogues of argentatin C (**1**−**4**) together with 10 known triterpenes (**5**−**14**) from the aerial parts of *P. incanum*, and evaluation of **1**−**4** for their potential antinociceptive activity.

RESULTS AND DISCUSSION

The crude extract of the aerial parts of *P. incanum* on fractionation by solvent-solvent partitioning, size-exclusion chromatography, and column chromatography followed by HPLC purification afforded four new (**1**−**4**) and 10 known (**5**−**14**) triterpenoids (Figure 1). The known triterpenoids were identified as argentatin A (**5**),[35,36] isoargentatin A (**6**),[35,37] 16-deoxyargentatin A (**7**),[35] 16-deoxyisoargentatin A (**8**),[35] 16-dehydroargentatin A (**9**) (previously obtained by chromium trioxide oxidation of argentatin A),[36a,38] argentatin B (**10**),[35,36] argentatin C (**11**),[35,36] 16-dehydroargentatin C (**12**),[35] quisquagenin (**13**),[35] and isoquisquagenin (**14**),[35] by comparison of their spectroscopic data with those reported.

Metabolite **1**, obtained as a colorless amorphous solid, was determined to have the molecular formula $C_{31}H_{52}O_4$ by a combination of HRESIMS, ^{13}C NMR, and HSQC data, indicating 6 degrees of unsaturation. The ^1H NMR spectrum of **1** (Table 1) exhibited six singlet methyls [δ_H 1.18 (H_3-18), 1.11 (H_3-26), 1.09 (H_3-29), 1.08 (H_3-27), 1.03 (H_3-28) and 0.87 (H_3-30)], a methyl doublet [δ_H 0.92 (J = 6.4 Hz, H_3-21)], two oxymethine protons [δ_H 4.46 (dt, J = 10.0, 4.8 Hz, H-16) and 3.65 (dd, J = 11.6, 3.2 Hz, H-24)], one OCH_3 [δ_H 3.21 (s)], and a pair of up-field doublets [δ_H 0.56 and 0.80 (AB, q, J = 4.4 Hz, H_2-19)] characteristic of nonequivalent protons of a cyclopropyl methylene group in cycloartane-type triterpenoids.[39] The ^{13}C NMR spectrum of **1** (Table 2), when analyzed with the help of HSQC data, revealed 31 signals due to a ketone carbonyl (δ_C 216.6), six quaternary carbons of which one is oxygenated (δ_C 77.2), six methines, including two

https://doi.org/10.1021/acsomega.3c02302
ACS Omega 2023, 8, 20085−20095

Table 1. ^{1}H NMR Spectroscopic Data of 1−4 and Argentatin C (11)

position	1	2	3	4	11
1	1.80 (m)	1.82 (m)	1.95 (m)	1.81 (dt,4.2, 13.2)	1.80 (dt,4.3, 13.2)
	1.55 (m	1.51 (m)	1.59 (m)	1.50 (m)	1.49 (m)
2	2.69 (td, 14.0, 6.4)	2.69 (dt, 6.4, 13.8)	2.57 (ddd, 7.0, 11.4, 15.8)	2.68 (dt, 6.4, 13.7)	2.66 (dt, 6.6, 13.9)
	2.29 (dt, 14.0, 2.4)	2.28 (ddd, 2.6, 4.4, 14.0)	2.40 (m)	2.26 (ddd, 13.7, 4.5, 2.7)	2.26 (ddd, 13.9, 4.7,2.3)
5	1.68 (m)	1.67 (m)	1.57 (m)	1.66 (dt, 12.7, 5.8)	1.66 (m)
6	1.55 (m)	1.55 (m)	1.61 (m)	1.53 (m)	1.54 (m)
	0.95 (m)	0.93 (dt, 2.0, 12.6)	1.02 (m)	0.93 (m)	0.94 (m)
7	1.32 (m)	1.38 (m)	2.05 (m)	1.35 (m)	1.35 (m)
	1.12 (m)	1.09 (m)	1.04 (m)	1.11 (m)	1.12 (m)
8	1.70 (m)	1.65 m		1.65 m)	1.68 (m)
11	2.06 (m)	2.05 (m)	2.04 (m)	2.02 (m)	2.03 (m)
	1.15 (m)	1.14 (m)	1.03 (m)	1.13 (m)	1.12 (m)
12	1.74 (m)	1.84 (m)	1.87 (m)	1.66 (dt, 12.7, 5.8)	2.00 (m)
	1.65 (m)	1.64 (m)	1.76 (m)	1.59 (dd, 12.7, 4.2)	1.14 (m)
15	2.02 (m)	2.03 (dd, 8.0, 13.1)	1.95 (m)	2.00 (m)	2.01 (m)
	1.35 (m)	1.47 (5.8, 13.1)	1.78 (m)	1.37 (brd, 12.2)	1.31 (m)
16	4.46 (ddd, 8.3, 7.2, 5.0)	4.58 (dt, 13.8, 7.5)	4.61 (dt, 13.8, 7.6)	4.46 (ddd, 12.2, 7.5, 4.7)	4.45 (dt, 10.0, 4.8)
17	1.60 (m)	1.81 (d, 8.4)	1.71 (d, 8.4)	1.61 (dd, 11.5, 4.7)	1.59 (m)
18	1.18 (s)	1.42 (s)	1.06 (s)	1.15 (s)	1.14 (s)
19	0.80 (d, 4.4)	0.80 (d, 4.4)	1.11 (s)	0.78 (d, 4.4)	0.78 (d, 4.4)
	0.56 (d, 4.4)	0.57 (d, 4.4)		0.56 (d, 4.4)	0.56 (d, 4.4)
20	1.92 (m)			1.81 (m)	1.87 (m)
21	0.92 (d, 6.4)	1.37 (s)	1.37 (s)	0.92 (d, 6.2)	0.88 (d, 6.4)
22	2.04 (m)	2.39 (dt, 4.6, 14.2)	2.37 (m)	1.72 (m)	1.60 (m)
	1.13 (m)	1.23 (m)	1.24 (m)	1.04 (m)	1.07 (m)
23	1.82 (m)	2.17 (dt, 4.6, 14.2)	2.17 (dt, 4.6, 14.2)	1.66 (m)	1.53 (m)
	1.08 (m)	1.77 (m)	177 (m)	1.21 (m)	1.36 (m)
24	3.65 (dd, 11.6, 3.2)	3.38 (brs)	3.37 (brs)	3.34 (d, 10.1)	3.51 (dd, 11.6, 2.8)
26	1.11 (s)	1.29 (s)	1.27 (s)	1.18 (s)	1.18 (s)
27	1.08 (s)	1.20 (s)	1.18 (s)	1.13 (s)	1.11 (s)
28	1.09 (s)	1.08 (s)	1.07 (s)	1.06 (s)	1.07 (s)
29	1.03 (s)	1.03 (s)	1.05 (s)	1.00 (s)	1.02 (s)
30	0.87 (s)	0.84 (s)	0.82 (s)	0.86 (s)	0.87 (s)
OMe	3.21 (s)				

oxygenated carbons (δ_C 72.4 and 73.8), 10 methylenes, seven methyls, and an OCH_3 carbon (δ_C 57.21). These data indicated that **1** is structurally related to argentatin C (**11**).[35,36b] In their ^{1}H and ^{13}C NMR spectra, the only difference between **1** and **11** was an additional singlet due to an OCH_3 group [δ_H 3.21 (s); δ_C 57.1 (CH_3)] in **1**. The molecular formula of **1** ($C_{31}H_{52}O_4$) indicated that compared to **11** ($C_{30}H_{50}O_4$), it has an additional CH_2 suggesting that one of the OH groups in **11** may have undergone methylation to an OCH_3 group in **1**. The observed heteronuclear multiple bond correlation (HMBC) correlation of the OCH_3 protons (δ_H 3.21) with the oxygenated quaternary carbon (δ_C 77.2, C-25) (Figure 2) confirmed that the OH group at C-25 in **11** has been replaced by an OCH_3 group in **1**. The coupling patterns of H-16 and H-24 suggested β-orientation for OH-16 and *R* configuration at C-24, respectively.[35] Thus, the structure of **1** was established as 25-dehydroxy-25-methoxyargentatin C [(16β,24*R*)-16,24-dihydroxy-25-methoxycycloartan-3-one].

The HRESIMS data of metabolite **2** exhibited a quasi-molecular ion peak at *m*/*z* 473.3601 (calcd for $C_{30}H_{49}O_4$ [M-H_2O+H]$^+$ 473.3631), suggesting the molecular formula $C_{30}H_{50}O_5$ and indicating 6 degrees of unsaturation. The ^{1}H NMR spectrum of **2** (Table 1) exhibited signals due to seven methyls and a pair of up-field doublets at δ_H 0.80 and 0.57 (*J* = 4.4 Hz) characteristic of geminal methylene protons of a tetra-substituted cyclopropane ring suggesting **2** to be a cycloartane-type triterpenoid.[39] The ^{13}C NMR spectrum of **2** (Table 2), when analyzed with the help of the HSQC data, indicated the presence of 30 carbons consisting of a ketone carbonyl (δ_C 216.5), seven quaternary carbons of which two are oxygenated (δ_C 78.6 and 76.0), five methines of which two are oxygenated (δ_C 73.8 and 69.7), 10 methylenes, and seven methyls. Since the carbonyl group accounted for only 1 degree of unsaturation, **2** should be pentacyclic. The ^{1}H and ^{13}C NMR spectroscopic data of **2** closely resembled those of argentatin C (**11**)[35,36b] (Tables 1 and 2), suggesting that **2** is an analogue of **11**. Comparison of the molecular formula of **2** ($C_{30}H_{50}O_5$) with that of **11** ($C_{30}H_{50}O_4$) indicated **2** to be an oxygenated analogue of **11**. The ^{1}H and ^{13}C NMR chemical shifts of the C-21 methyl group of **2** (δ_H 1.37; δ_C 27.1) compared to those of **11** (δ_H 0.88; δ_C 17.7) indicated that this methyl is attached to an oxygenated carbon.[40] This was further confirmed by the HMBC correlation of H_3-21 to C-20 (Figure 2). Based on their ^{13}C NMR chemical shifts, β-orientation for OH-16 and *S* configuration for C-20 were assigned.[40a] The ^{13}C NMR chemical shift of C-21 (δ_C 27.1) further supported the *S* configuration of C-20.[41] The absolute configuration of the chiral center at C-24 of **2** was determined to be *R* by the application of the advanced Mosher's ester method (Figure 3).[42] Metabolite **2** was thus identified as 20*S*-hydroxyargenta-

https://doi.org/10.1021/acsomega.3c02302
ACS Omega 2023, 8, 20085−20095

Table 2. ^{13}C NMR Spectroscopic Data of 1−4 and Argentatin C (11)

position	1	2	3	4	11
1	33.5 CH_2	33.3 CH_2	35.8 CH_2	33.4 CH_2	33.3 CH_2
2	37.5 CH_2	37.5 CH_2	34.6 CH_2	37.5 CH_2	37.4 CH_2
3	216.6 C	216.5 C	217.7 C	216.6 C	216.6 C
4	50.2	50.2 C	47.4 C	50.2 C	50.2 C
5	48.5 CH	48.5 CH	51.2 CH	48.5 CH	48.4 CH
6	21.4 CH_2	21.4 CH_2	19.3 CH_2	21.4 CH_2	21.4 CH_2
7	26.1 CH_2	25.9 CH_2	26.2 CH_2	25.9 CH_2	25.9 CH_2
8	47.9 CH	47.5 CH	134.3 C	47.6 CH	47.5 CH
9	20.8 C	20.6 C	133.3 C	20.9 C	20.8 C
10	25.9 C	26.2 C	36.9 C	26.1 C	25.9 C
11	26.4 CH_2	26.5 CH_2	20.8 CH_2	26.4 CH_2	26.0 CH_2
12	32.7 CH_2	33.5 CH_2	31.9 CH_2*	32.6 CH_2	32.5 CH_2
13	45.3 C	46.2 C	45.3 C*	45.3 C	45.3 C
14	46.5 C	46.3 C	47.2 C*	46.8 C	46.6 C
15	47.9 CH_2	48.4 CH_2	43.9 CH_2	47.7 CH_2	47.8 CH_2
16	72.4 CH	73.8 CH	74.1 CH	72.8 CH	72.7 CH
17	57.1 CH	58.6 CH	57.1 CH	57.0 CH	56.7 CH
18	18.9 CH_3	21.5 CH_3	19.2 CH_3	20.0 CH_3	18.9 CH_3
19	29.8 CH_2	30.2 CH_2	18.4 CH_3	29.8 CH_2	29.8 CH_2
20	26.5 CH	78.6 C	78.4 C	31.5 CH	26.3 CH
21	17.7 CH_3	27.1 CH_3	27.6 CH_3	18.5 CH_3	17.7 CH_3
22	26.4 CH_2	27.2 CH_2	27.1 CH_2	33.8 CH_2	26.4 CH_2
23	31.4 CH_2	22.5 CH_2	22.5 CH_2	28.6 CH_2	31.1 CH_2
24	73.8 CH	69.7 CH	69.6 CH	80.3 CH	75.2 CH
25	77.2 C	76.0 C	76.0 C	73.2 C	73.0 C
26	25.6 CH_3	27.4 CH_3	27.4 CH_3	23.1 CH_3	22.8 CH_3
27	25.9 CH_3	28.1 CH_3	28.1 CH_3	26.6 CH_3	26.8 CH_3
28	20.8 CH_3	20.8 CH_3	26.1 CH_3	20.8 CH_3	20.7 CH_3
20	22.2 CH_3	22.1 CH_3	21.3 CH_3	22.2 CH_3	22.1 CH_3
30	20.0 CH_3	19.9 CH_3	24.9 CH_3	19.0 CH_3	19.9 CH_3
OMe	57.1 CH_3				

tin C [(16β,20S,24R)-16,20,24,25-tetrahydroxycycloarten-3-one].

The HRESIMS, ^{1}H, and ^{13}C NMR spectroscopic data of **3** were consistent with the molecular formula $C_{30}H_{50}O_5$, indicating 6 degrees of unsaturation. In its ^{1}H NMR spectrum (Table 1), **3** exhibited signals due to eight methyl groups, suggesting it to be a lanostane-type triterpenoid.[35] The ^{13}C NMR spectrum of **3**, when analyzed with the help of HSQC data, revealed 30 carbon signals including a carbonyl carbon (δ_C 217.7), seven quaternary carbons of which two are olefinic (δ_C 134.3 and 133.3) and two are oxygenated (δ_C 78.4 and 76.0), four methines of which two are oxygenated (δ_C 74.1 and 69.6), nine methylenes, and eight methyls. Since the carbonyl group and the double bond accounted for 2 degrees of unsaturation, **3** should be tetracyclic. These data revealed that the structure of **3** is closely related to that of the known lanostane triterpenoid, isoargentatin C (**15**).[35] The molecular weight difference of 16 Da between **3** and **15** suggested that **3** is an oxygenated analogue of **15**. The major difference in their NMR data was found to be the absence of the methyl doublet (δ_H 0.93) in **3**, which was assigned to H_3-21 in **15**. Instead, **3** showed a singlet (δ_H 1.37) due to a methyl group attached to an oxygenated carbon (δ_C 78.4), suggesting the presence of an OH group at C-20. This was confirmed by the presence of an HMBC correlation between H_3-21 and C-20 (Figure 2). Based on their ^{13}C NMR chemical shifts, OH-16 was determined to have β-orientation and C-20 to have S configuration.[40a] The coupling pattern of H-24 and the chemical shift of C-24 were found to be similar to those of 20S-hydroxyargentatin C (**2**) (see above), suggesting the R absolute configuration for C-24. Thus, metabolite **3** was identified as 20S-hydroxyisoargentatin C [(16β,20S,24R)-16,20,24,25-tetrahydroxylanost-8-en-3-one].

Metabolite **4** exhibited a $[M + Na]^+$ ion at m/z 497.3604 in its HRESIMS, consistent with the molecular formula $C_{30}H_{50}O_4$ which is the same as that of argentatin C (**11**). The ^{1}H and ^{13}C NMR spectroscopic data of **4** were similar to those of **11** (Tables 1 and 2), except for some signals of the side-chain moiety.[35,36b] Argentatin C (**11**) contains a 24β,25-dihydroxylated side-chain moiety. The HMBC spectrum of **4** (Figure 2) suggested that it also contains a 24,25-dihydroxylated side chain as in **11**. However, in their ^{13}C NMR spectra, the signals due to the OH-24 bearing carbon (C-24) of **4** and **11** appeared at δ_C 80.3 and δ_C 75.2 ppm, respectively, suggesting that they have different configurations at C-24. Since the configuration of C-24 in **11** is known to be R,[35,36] the configuration of this carbon in **4** was suspected to be S, and this was confirmed by the application of the advanced Mosher's ester method (Figure 3).[42] Hence, metabolite **4** was identified as 24-*epi*-argentatin C [(16β,24S)-16,24,25-trihydroxycycloarten-3-one].

We have previously shown that the crude MeOH/CH_2Cl_2 (1:1) extract of *P. incanum* and one of its major metabolites, argentatin C (**11**), exhibit antinociceptive activity by inhibiting depolarization-evoked calcium influx.[10] In addition, **11** decreased excitability as well as inhibited the current through VGSC and low-voltage-activated calcium channels in rat DRG neurons, whereas the other major metabolites of this extract, argentatin A (**5**), argentatin B (**10**), and isoargentatin A (**6**), had no effect on these neurons.[10] In the current study, the excitability of DRG neurons was tested in the presence of argentatin C (**11**) and its analogues (**1**−**4**). Compounds **1**−**4** and **11** were acutely incubated with DRG neurons in order to evaluate if these compounds could modulate the excitable properties of these cells which is attributed to VGSCs and VGCCs of rat DRG neurons. The isolated neurons were incubated in the presence of 20 μM of each analogue for 15 min prior to recording and in the external solution during recording. Argentatin C (**11**) served as an internal positive control. As reported previously, **11** significantly decreased the number of action potentials (APs) observed in response to

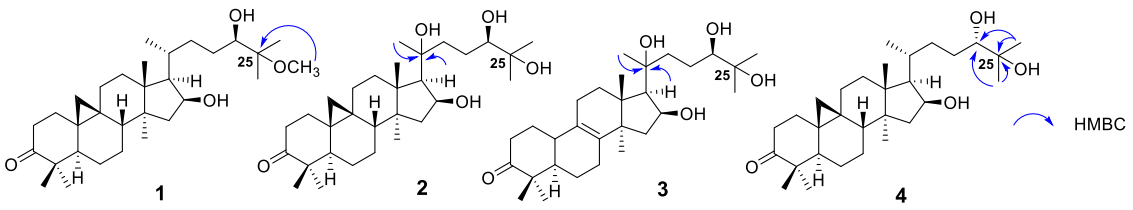

Figure 2. Key HMBC correlations of **1**−**4**.

https://doi.org/10.1021/acsomega.3c02302
ACS Omega 2023, 8, 20085−20095

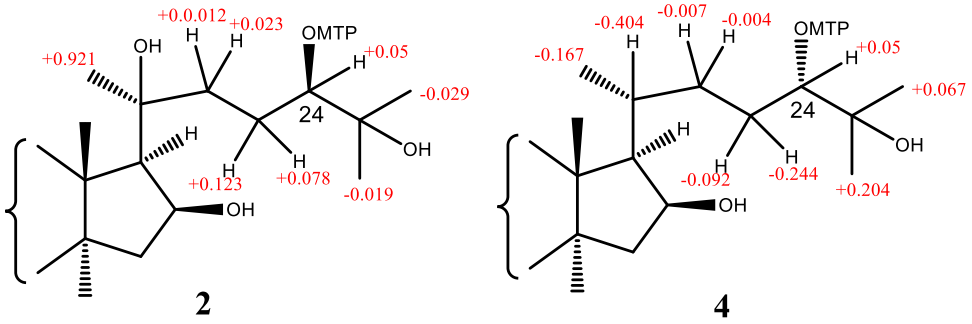

Figure 3. $\Delta\delta$ values [$\Delta\delta$ values (in ppm) = $\delta_S - \delta_R$] obtained for (*S*)- and (*R*)-MTPA esters of **2** and **4**.

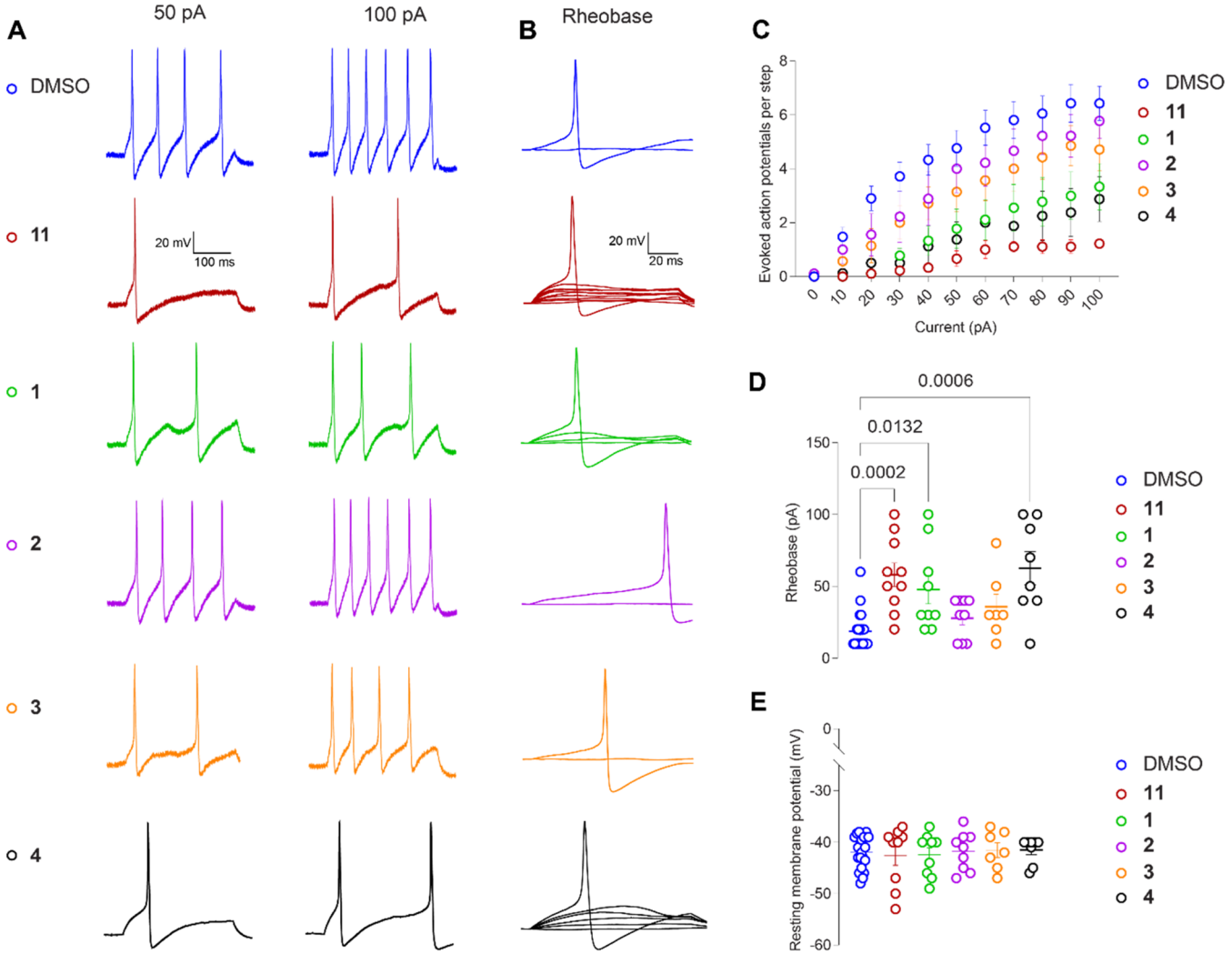

Figure 4. Inhibition of excitability in rat dorsal root ganglion (DRG) neurons by argentatin C (**11**) and its analogues **1**−**4**. (A) Representative traces of action potentials displayed by DRG neurons in culture after incubation with dimethyl sulfoxide (DMSO) or 20 μM **11** and **1**−**4** in response to current injections at 50 and 100 pA for 300 ms. Representative traces (B) and quantification of the rheobase (D) [i.e., current required for eliciting the first action potential (AP)] showing significant increase in the presence of **11** and **1** when compared with DMSO. (C) Quantification of the number of action potentials evoked in response to current injection (see Table S1; Supporting Information). (E) Resting membrane potential (see Table S2; Supporting Information). [Error bars indicate mean ± SEM, *p* values as indicated (n = 9−10 cells). Kruskal−Wallis test].

each step of injected current (Figure 4A,C and Table S1).[10] 25-Dehydroxy-25-methoxyargentatin C (**1**) and 24-*epi*-argentatin C (**4**) also inhibited the number of APs, whereas the excitability of rat DRG neurons in the presence of 20*S*-hydroxyargentatin C (**2**) and 20*S*-hydroxyisoargentatin C (**3**) remained unaffected (Figure 4C and Table S1). Argentatin C (**11**) and its analogues **1** and **4** also increased the rheobase, defined as the minimum current necessary to evoke an AP as indicated by the following data compared to the negative control (0.1% DMSO 18.57 ± 2.79): argentatin C (**11**) 58.0 ± 8.14; 25-dehydroxy-25-methoxyargentatin C (**1**) 47.8 ± 9.97; 20*S*-hydroxyargentatin C (**2**) 27.78 ± 4.65; 20*S*-hydroxyisoar-

https://doi.org/10.1021/acsomega.3c02302
ACS Omega 2023, 8, 20085−20095

gentatin C (**3**) 35.71 ± 8.69; and 24-*epi*-argentatin C (**4**) 62.5 ± 11.61 (Figure 4B,D). Additionally, the resting membrane potential—an important mechanism regulating excitability—remained unchanged between conditions (Figure 4E and Table S2). Our results show that 25-dehydroxy-25-methoxyargentatin C (**1**), 24-*epi*-argentatin C (**4**), and argentatin C (**11**) diminished the excitability of rat DRG neurons. A summary of preliminary structure−activity relationship (SAR) data for argentatin C and its analogues is depicted in Figure 5. As the

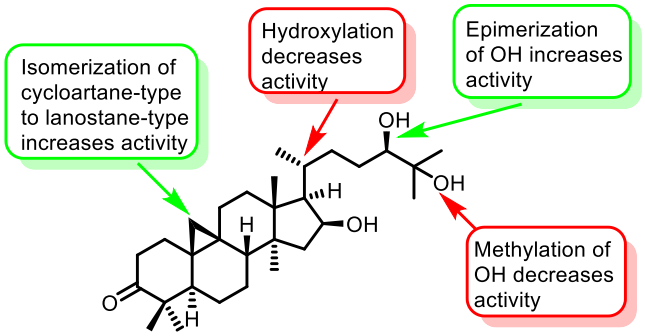

Figure 5. Summary of structure−activity relationships of argentatin C analogues for inhibition of excitability in rat dorsal root ganglion (DRG) neurons.

excitability depends on part of the activity of VGSCs and VGCCs, these results strongly suggest that like argentatin C (**11**), its analogues **1** and **4** inhibit these channels.[10] However, behavioral experiments in animal models with acute or chronic pain will be necessary to determine if these compounds could alleviate pain.

As we did previously for argentatin C (**11**),[10] we used *in silico* docking to predict the binding sites for its analogues **1**−**4** to pain-relevant VGSCs and VGCCs. Our previous analysis identified the hydrophobic fenestrations and central pore as significantly more likely to be the sites of binding for **11**,[10] so the analogues were docked at these locations as well. In the VGSCs, the five compounds are predicted to dock to the pore and a single fenestration: fenestration III−IV in NaV1.7 and NaV1.8 and fenestration II−III in NaV1.9 (Figure 6A). For the VGCC targets, the predictions were split between the pore and two fenestrations in each case (Figure 6B). These results confirm that the argentatin C analogues are able to bind to the VGSC and VGCC fenestrations. These hydrophobic access channels were predicted over 40 years ago by Hille as important antinociceptive drug access pathways.[43] Further, an increasing number of compounds have been found to utilize one or more fenestrations to anchor compounds within the pore of both VGSC (e.g., flecainide,[44] bulleyaconitine A,[45] XEN907 and TC-N1752,[46] and A-803467[47]) and VGCC (e.g., Z944,[48] cinnazarine,[49] PD173212,[50] mibefradil, otilonium bromide, and pimozide[51]) channels. Notably, the natural product bulleyaconitine A,[52] as well as TC-N1752,[53] A-803467,[54] Z994,[55] and CaV2.2 blocker 1[56] have been shown to have analgesic properties, supporting the fenestrations as sites that can be targeted for the development of more effective pain therapeutics. Unfortunately, the moderate resolution of the currently available cryoEM structures and inherent uncertainties of homology modeling lead to ambiguities in amino acid side-chain placement which likely has led to the highly similar docking scores (Table S3) and predicted contacts, precluding further interpretation of our docking results for argentatin C (**11**) and its analogues **1**−**4**.

EXPERIMENTAL SECTION

General Experimental Procedures. Optical rotations were measured in CH_3OH with a JASCO Dip-370 digital polarimeter. One-dimensional (1D) and two-dimensional (2D) NMR spectra were recorded in $CDCl_3$ and pyridine-d_5

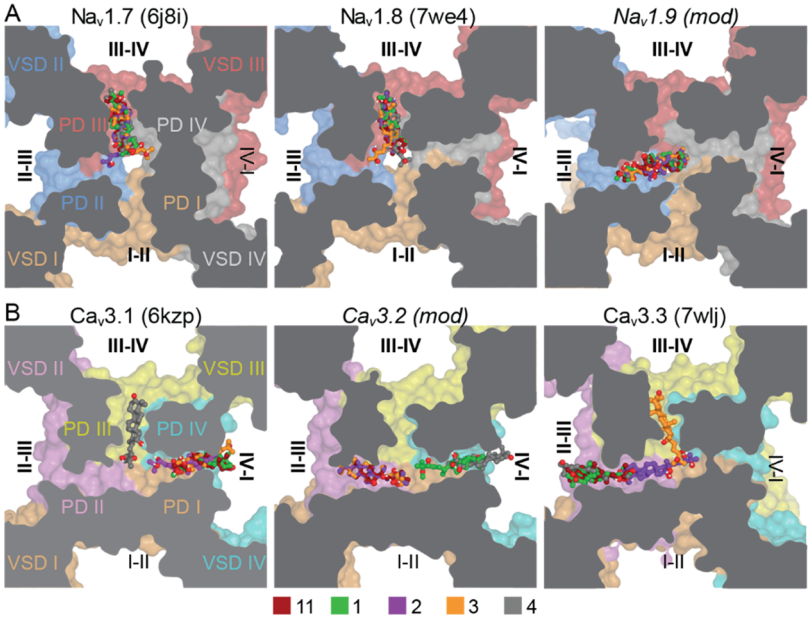

Figure 6. Predicted binding sites of argentatin C (**11**) and analogues **1**−**4** in pain-relevant VGSCs and VGCCs. Docking poses for (A) VGSCs and (B) VGCCs. Top docked poses are shown as sticks with carbon atoms colored as labeled in legend, oxygen in red, and polar hydrogen in white. Channels are shown in surface representation, sliced at the level of the fenestrations (viewed from the extracellular side) and colored by domain as indicated (PD, pore domain; VSD, voltage-sensing domain). Fenestrations are labeled with the Roman numerals of the adjacent pore domains with bold text denoting open fenestrations.

https://doi.org/10.1021/acsomega.3c02302
ACS Omega 2023, 8, 20085−20095

with a Bruker Avance III 400 spectrometer at 400 MHz for ^{1}H NMR and 100 MHz for ^{13}C NMR using residual solvent resonances ($CDCl_3$: ^{1}H NMR, 7.24; ^{13}C NMR, 77.0; pyridine-d_5: ^{1}H NMR, 8.74, 7.58, 7.22; ^{13}C NMR, 150.4, 135.9, 123.9) as internal references. The ^{1}H NMR spectra of Mosher's esters were recorded in pyridine-d_5 with a Bruker DRX-500 spectrometer at 500 MHz. The chemical shift (δ) values are given in parts per million (ppm), and the coupling constants (J values) are in hertz. High-resolution mass spectra (HRMS) were recorded on a JEOL HX110A spectrometer. Circular dichroism (CD) spectra were obtained using a Jasco J-810 spectropolarimeter. Gel permeation chromatography was carried out using a Sephadex LH-20 (GE-Healthcare Bio-Sciences AB, Uppsala, Sweden). Normal-phase (NP) column chromatography was performed using Baker silica gel 40 μm flash chromatography packing (J. T. Baker), and reversed-phase (RP) chromatography was carried out using BAKER-BOND C_{18} 40 μm preparative LC packing (J. T. Baker). Analytical thin-layer chromatography (TLC) was performed on aluminum-backed precoated 0.25 mm silica gel 60 F_{254} plates (Merck, Darmstadt, Germany), and spots were visualized under UV light and spraying with a solution of anisaldehyde in H_2SO_4/HOAc followed by heating. HPLC purifications were carried out on a 10 × 250 mm Phenomenex Luna 5 μm C_{18} column (3 mL/min flow rate) with a Waters Delta Prep system consisting of a PDA 996 detector.

Plant Material. Aerial parts of *P. incanum* were collected by Dr. Steven P. McLaughlin of the University of Arizona (collection no. 7043) on Sept. 14, 1996, in Pima County (Old Highway, 83 SE of junction with Interstate I-10; 31 59.67′ N, 110 40.35′ W, elevation ca. 4,000 feet). A voucher sample has been deposited at the University of Arizona Herbarium (Catalog No. ARIZ 336215).

Extraction of *P. incanum*. Freshly collected aerial parts of *P. incanum* were air-dried and powdered, and a portion (638.0 g) of this material was extracted with $CHCl_3$-CH_3OH (1:1) at room temperature for 24 h. After filtration, the resulting filtrate was concentrated below 40 °C and under reduced pressure to afford the crude extract (137.0 g), which was stored in a sealed bottle at −5 °C until use.

Isolation and Identification of Metabolites. A portion (10.0 g) of the above extract was partitioned between hexanes and 80% aq CH_3OH. The 80% aq CH_3OH layer was then diluted to 50% aq CH_3OH with water and extracted with $CHCl_3$. The resulting solutions were evaporated separately under reduced pressure to afford hexanes (4.43 g), $CHCl_3$ (2.64 g), and 50% aq CH_3OH (2.29 g) fractions. A portion (4.3 g) of the hexanes fraction was subjected to gel permeation chromatography on a column of Sephadex LH-20 (200.0 g) made up in hexanes/CH_2Cl_2 (1:4) and eluted with hexanes/CH_2Cl_2 (1:4) followed by CH_3OH. Twenty-four fractions were collected, and fractions having similar TLC profiles were combined to give six major fractions [A (0.44 g), B (1.69 g), C (1.47 g), D (0.16 g), E (0.19 g), and F (0.65 g)]. Fraction B (1.60 g) was chromatographed over a column of silica gel (30.0 g) made up in hexanes and eluted with 200.0 mL each of hexanes, hexanes/$CHCl_3$ (2:1), $CHCl_3$ followed by $CHCl_3$/CH_3OH (95:5). Sixteen subfractions were collected [B1 (15.7 mg), B2 (15.1 mg), B3 (1.6 mg), B4 (2.6 mg), B5 (4.5 mg), B6 (4.0 mg), B7 (3.6 mg), B8 (11.2 mg), B9 (86.0 mg), B10 (101.1 mg), B11 (67.7 mg), B12 (57.0 mg), B13 (178.2 mg), B14 (58.1 mg), B15 (930.8 mg), and B16 (35.6 mg)]. The major fraction B15 (930.0 mg) containing triterpenoids was re-chromatographed over a column of silica gel (30.0 g) made up in $CHCl_3$ and eluted with $CHCl_3$, $CHCl_3$/CH_3OH (99.5:0.5), $CHCl_3$/CH_3OH (99:1), followed by $CHCl_3$/CH_3OH (95:5) to give nine subfractions ($B15_A$−$B15_I$). Subfraction $B15_B$ (467.7 mg) was further separated by RP C_{18} (18.0 g) column chromatography using CH_3OH/H_2O (90:10) followed by CH_3OH as eluant to give six subfractions ($B15_{B1}$−$B15_{B6}$). Subfraction $B15_{B2}$ (53.6 mg) on purification by reversed-phase high-performance liquid chromatography (RP-HPLC) afforded argentatin B [**10**, 31.1 mg, t_R 33.0 min, CH_3OH/H_2O (98:2)]. RP-HPLC purification of the subfraction $B15_{B3}$ (64.9 mg) using CH_3OH/H_2O (98:2) as the mobile phase yielded 16-dehydroargentatin A (**9**, 2.2 mg, t_R 32.0 min), 16-deoxyisoargentatin A (**8**, 3.1 mg, t_R 37.5 min), 16-deoxyargentatin A (**7**, 8.2 mg, t_R 44.0 min), and an additional amount of argentatin B (**10**, 16.8 mg, t_R 35.0 min). RP-HPLC purification of the combined subfractions $B15_D$ (29.4 mg) and $B15_E$ (31.3 mg) afforded an additional amount of 16-dehydroargentatin A (**7**, 12.6 mg). Purification of the subfraction $B15_F$ (53.3 mg) by RP-HPLC followed by silica gel column chromatography gave 16-dehydroargentatin C (**12**, 2.2 mg), 25-dehydroxy-25-methoxyargentatin C (**1**, 1.7 mg), 20*S*-hydroxyargentatin C (**2**, 1.4 mg), and 20*S*-hydroxyisoargentatin C (**3**, 1.5 mg). Further purification of the subfraction $B15_G$ (24.1 mg) by RP-HPLC yielded argentatin A (**5**, 1.4 mg) and isoargentatin A (**6**, 0.8 mg).

The $CHCl_3$ fraction (2.5 g) obtained above was subjected to size-exclusion chromatography over Sephadex LH-20 (300.0 g) made up in hexanes/CH_2Cl_2 (1:4) and eluted with 1.0 L each of hexanes/CH_2Cl_2 (1:4), CH_2Cl_2/acetone (4:1), CH_2Cl_2/acetone (2:3) followed by CH_3OH. Ninety-three fractions were collected, and fractions having similar TLC profiles were combined to give nine major fractions [C1 (455.8 mg), C2 (213.2 mg), C3 (149.7 mg), C4 (168.4 mg), C5 (378.0 mg), C6 (278.9 mg), C7 (243.6 mg), C8 (202.5 mg), and C9 (439.6 mg)]. Fraction C2 (213 mg) on further purification by RP C_{18} (20.0 g) column chromatography using combinations of CH_3OH and H_2O gave argentatin C (**11**, 19.8 mg). Fraction C3 (145 mg) was re-chromatographed over a column of RP C_{18} (18.0 g) made up in CH_3OH/H_2O (80:20) and eluted with CH_3OH/H_2O (80:20), CH_3OH/H_2O (80:20), and CH_3OH. Twenty-four fractions were collected and combined according to their TLC profile to give 10 subfractions [(C3A (11.0 mg), C3B (8.8 mg), C3C (6.1 mg), C3D (12.5 mg), C3E (5.8 mg), C3F (12.1 mg), C3G (25.5 mg), C3H (28.7 mg), C3I (9.4 mg), and C3J (18.4 mg)]. Purification of the subfraction C3H (28.7 mg) by RP-C_{18} HPLC [CH_3OH/H_2O (92.5:7.5, v/v, 3 mL/min)] gave 24-*epi*-argentatin C (**4**, 15.2 mg, t_R = 23.5 min) as a white amorphous solid. The subfraction C3J was found to consist of an inseparable mixture of quisquagenin (**13**) and isoquisquagenin (**14**) in a ratio of 1:2 by careful analyses of its ^{1}H and ^{13}C NMR data (Figure S19).[35]

*25-Dehydroxy-25-methoxyargentatin C [(16β,24R)-16,24-dihydroxy-25-methoxycycloartan-3-one] (**1**).* Amorphous white solid: $[\alpha]_D^{25}$ +39 (*c* 0.16, CH_3OH); ECD (CH_3OH) [θ] −23,282 (300 nm); ^{1}H NMR data; see Table 1; ^{13}C NMR data; see Table 2; positive HRESIMS *m*/*z* 511.3761 [M + Na]$^+$ (calcd for $C_{31}H_{52}O_4Na$ 511.3763).

*20S-Hydroxyargentatin C [(16β,20S,24R)-16,20,24,25-tetrahydroxycycloartan-3-one] (**2**).* Amorphous white solid: $[\alpha]_D^{25}$ +51 (*c* 0.14, CH_3OH); ECD (CH_3OH) [θ] 16,378 (205 nm); ^{1}H NMR data; see Table 1; ^{13}C NMR data; see

https://doi.org/10.1021/acsomega.3c02302
ACS Omega 2023, 8, 20085−20095

Table 2; positive HRESIMS m/z 473.3601 $[MH-H_2O]^+$ (calcd for $C_{30}H_{49}O_4$ 473.3631).

*20S-Hydroxyisoargentatin C [(16β,20S,24R)-16,20,24,25-tetrahydroxylanost-8-en-3-one] (**3**).* Amorphous white solid: $[\alpha]_D^{25}$ +17 (c 0.14, CH_3OH); ECD (CH_3OH) [θ] −2217 (296 nm); ^{1}H NMR data; see Table 1; ^{13}C NMR data; see Table 2; positive HRESIMS m/z 513.3565 $[M + Na]^+$ (calcd for $C_{30}H_{50}O_5Na$ 513.3556).

*24-Epi-argentatin C [(16β,24S)-16,24,25-trihydroxycycloartan-3-one] (**4**).* Amorphous white solid: $[\alpha]_D^{25}$ +18 (c 0.12, CH_3OH); ECD (CH_3OH) [θ] 1449 (223 nm), −527 (300 nm); ^{1}H NMR data; see Table 1; ^{13}C NMR data; see Table 2; positive HRESIMS m/z 497.3604 $[M + Na]^+$ (calcd for $C_{30}H_{50}O_4Na$ 497.3607).

Preparation of (*S*)- and (*R*)-MTP Ester Derivatives of 2, and 4 by Advanced Mosher's Ester Procedure. Each compound (1.5 mg) was transferred into a clean NMR tube and was dried completely *in vacuo*. Pyridine-d_5 (1.0 mL) and (*R*)-(−)-α-methoxy-α-trifluoromethylphenylacetyl chloride (5.0 μL) were added into the NMR tube immediately under a stream of N_2, and then the NMR tube was shaken carefully to mix the sample and the MTPA chloride evenly. The reaction in the NMR tube was monitored by ^{1}H NMR and left at 25 °C for 2 h to give the (*S*)-MTPA derivatives (**2a** and **4a**). Additional portions of **2** and **4** (1.5 mg each) in pyridine-d_5 (1.0 mL) were reacted in a second NMR tube with (*S*)-(+)-α-methoxy-α-trifluoromethylphenylacetyl chloride (5.0 μL) at 25 °C for 2 h to afford the (*R*)-MTPA derivatives (**2b** and **4b**). ^{1}H NMR data of **2a** (500 MHz, pyridine-d_5): δ 5.138 (1H, brt, J = 3.1 Hz, H-24), 2.315 (1H, dd, J = 14.8, 2.8 Hz, Ha-23), 1.915 (1H, dd, J = 14.8, 3.2 Hz, Hb-23), 1.616 (3H, s, H_3-21), 1.430 (3H, s, H_3-26), 1.308 (3H, s, H_3-27), 1.298 (1H, m, Ha-22), 1.021 (1H, m, Hb-22). ^{1}H NMR data of **2b** (500 MHz, pyridine-d_5): δ 5.088 (1H, brt, J = 3.1, H-24), 2.192 (1H, dd, J = 14.6, 3.0 Hz, Ha-23), 1.837 (1H, dd, J = 14.6, 2.9 Hz, Hb-23), 1.595 (3H, s, H_3-21), 1.449 (3H, s, H_3-26), 1.337 (1H, s, H_3-27), 1.286 (1H, m, Ha-22), 0.998 (1H, m, Hb-22). ^{1}H NMR data of **4a** (500 MHz, pyridine-d_5): δ 5.635 (1H, dd, J = 9.9, 2.2 Hz, H-24), 2.183 (1H, m, Ha-23), 1.963 (1H, m, H-17), 1.949 (1H, m, H-20), 1.905 (Hb-23), 1.727 (1H, m, Ha-22), 1.666 (3H, s, H_3-26), 1.483 (3H, s, H_3-18), 1.445 (3H, s, H_3-27), 1.437 (1H, m, Hb-22), 0.959 (3H, d, J = 6.2 Hz, H_3-21), 0.951 (3H, s, H_3-30). ^{1}H NMR data of **4b** (500 MHz, pyridine-d_5): δ 5.597 (1H, d, J = 9.2 Hz, H-24), 2.427 (1H, m, Ha-23), 2.353 (1H, m, Ha-22), 1.997 (1H, m, Hb-23), 1.734 (1H, m, Ha-22), 1.462 (3H, s, H_3-26), 1.441 (1H, m, Hb-22), 1.378 (3H, s, H_3-27), 1.126 (3H, d, J = 6.2 Hz, H_3-21).

Animals. Pathogen-free adult female Sprague−Dawley rats (100−200 g, Charles River Laboratories, Wilmington, MA) were kept in light (12 h light, 12 h dark cycle) and temperature (23 ± 3 °C) controlled rooms. Water and standard rodent diet were available ad libitum. All animal use was conducted in accordance with the National Institutes of Health guidelines, and the study was conducted in strict accordance with recommendations in the Guide for the Care and Use of Laboratory Animals of the New York University (Protocol No.: PROTO202100104). All animals were housed and bred at the Kriser Dental Center Animal Facility of the University of New York. Efforts were made to minimize animal suffering.

Electrophysiology. As previously described, dorsal root ganglia (DRG) were collected and dissociated from female Sprague−Dawley rats, aged 4−6 weeks old.[10] Compounds were applied for 15 min before and during the recording at 20 μM using 0.1% DMSO as a vehicle control. The excitability was tested in response to current injection between 0 and 100 pA with increments of 10 pA in the presence of 0.1% DMSO (control), or 20 μM of **11**, **1**, **2**, **3**, or **4**. The external solution was composed of NaCl (154 mM), KCl (5.6 mM), $CaCl_2$ (2 mM), $MgCl_2$ (1 mM) D-glucose (10 mM), HEPES (8 mM), pH 7.4 and 319 milliOsmol/L. The internal solution consisted of KCl (137 mM), NaCl (10 mM), $MgCl_2$ (1 mM), EGTA (1 mM), HEPES (10 mM), pH = 7.3 and 305 milliOsmol/L.

Homology Modeling and Ligand Docking. As previously reported,[10] the Baker Lab's structure prediction server[57] was used to generate homology models for the α subunit of human NaV1.9 (UniProt ID Q9UI33-1) based on the structure of NaV1.7 with TTX bound (PDB 6j8i[58]) and for human CaV3.2 (UniProt ID O95180-1) based on the structure of CaV3.1 with Z944 bound (PDB 6kzp[48]). Briefly, 10 models were sampled for each target. Models with the lowest error estimates and the same number of open fenestrations as the template were selected for docking and trimmed to remove unreliably modeled intracellular loops prior to docking. Protein and ligand preparation and docking were conducted using Schrödinger Docking Suite tools.[59] Argentatin C (**11**) and its analogues **1**−**4**, and Z944 were prepared from isomeric SMILES strings using LigPrep[59] with possible ionization states at pH 7.0. The cryoEM structure of human NaV1.7 (PDB 6j8i[58]), NaV1.8 (PDB 7we4[47]), CaV3.1 (PDB 6kzp[48]), CaV3.3 (PDB 7wLj[51]), and the trimmed homology models of NaV1.9 and CaV3.2 were prepared using the Protein Preparation Wizard,[60] and the charges on K1462 (canonical K1865) in PDB 6kzp, K1503 in the CaV3.2 model, and K1379 in PDB 7wLj were manually adjusted from +1 to 0 prior to docking. Our previous work identified the central pore and fenestrations as the most likely binding site for **11**,[10] so we selected the same grid location for docking its analogues **1**−**4** with an enclosing box at the centroid of residues N388, F956, V1505, and V1820, and expanded the ligand-midpoint box to 32x32x32 Å^3 to completely enclose the fenestrations. Docking was performed with Glide Standard Precision (SP) mode[61] with enhanced sampling to obtain up to 10 poses at each site. We previously showed that redocking of Z944 to the prepared PDB 6kzp reproduced the bound pose (not shown) with a docking score of −6.6 kcal/mol.[10] Docking scores for **11** and its analogues **1**−**4** were generally not significantly different at each target, precluding interpretation (average of top scores in kcal/mol: −7.3 ± 0.1 for NaV1.7, −6.9 ± 0.2 for NaV1.8, −6.6 ± 0.2 for NaV1.9, −6.5 ± 0.6 for CaV3.1, −7.1 ± 0.8 for CaV3.2, −5.2 ± 0.3 for CaV3.3). The top pose at each site was selected for visualization. Figure 6A,B was generated with PyMOL.[62]

■ ASSOCIATED CONTENT

Supporting Information

The Supporting Information is available free of charge at https://pubs.acs.org/doi/10.1021/acsomega.3c02302.

^{1}H, ^{13}C, and 2D NMR, ECD, and HREIMS spectra of **1**−**4**; statistical summary of excitability of rat DRG neurons toward **11** and **1**−**4**; and resting membrane potential and docking scores of **11** and **1**−**4** (PDF)

https://doi.org/10.1021/acsomega.3c02302
ACS Omega 2023, 8, 20085−20095

AUTHOR INFORMATION

Corresponding Authors

Rajesh Khanna − *NYU Pain Research Center and Department of Molecular Pathobiology, College of Dentistry, New York University, New York, New York 10010, United States; Department of Neuroscience and Physiology and Neuroscience Institute, School of Medicine, New York University, New York, New York 10010, United States;* orcid.org/0000-0002-9066-2969; Phone: +1 520 271 0433; Email: rk4272@nyu.edu

A. A. Leslie Gunatilaka − *Southwest Center for Natural Products Research, School of Natural Resources and the Environment, College of Agriculture and Life Sciences, University of Arizona, Tucson, Arizona 85719, United States;* orcid.org/0000-0001-9663-3600; Phone: +1 520 621 9932; Email: leslieg1@email.arizona.edu; Fax: +1 520 621 8378

Authors

Ya-ming Xu − *Southwest Center for Natural Products Research, School of Natural Resources and the Environment, College of Agriculture and Life Sciences, University of Arizona, Tucson, Arizona 85719, United States*

E. M. Kithsiri Wijeratne − *Southwest Center for Natural Products Research, School of Natural Resources and the Environment, College of Agriculture and Life Sciences, University of Arizona, Tucson, Arizona 85719, United States*

Aida Calderon-Rivera − *NYU Pain Research Center and Department of Molecular Pathobiology, College of Dentistry, New York University, New York, New York 10010, United States*

Santiago Loya-López − *NYU Pain Research Center and Department of Molecular Pathobiology, College of Dentistry, New York University, New York, New York 10010, United States*

Samantha Perez-Miller − *NYU Pain Research Center and Department of Molecular Pathobiology, College of Dentistry, New York University, New York, New York 10010, United States*

Complete contact information is available at: https://pubs.acs.org/10.1021/acsomega.3c02302

Notes

The authors declare the following competing financial interest(s): RK is the co-founder of Regulonix LLC, a company developing non-opioid drugs for chronic pain and ElutheriaTx Inc., a company developing gene therapy approaches for chronic pain. All other authors declare no competing financial interests.

ACKNOWLEDGMENTS

Financial support for this work from National Institute of Neurological Disorders and Stroke (NS098772 and NS120663) and National Institute of Drug Abuse (DA042852) to R.K. is gratefully acknowledged. The authors thank Professor L.-J. Xuan, Shanghai Institute of Materia Medica, Chinese Academy of Sciences, for providing HRMS data.

REFERENCES

(1) Powell, A. M. *Trees and Shrubs of the Trans-Pecos and Adjacent Areas*; University of Texas Press: Austin, Texas. 1998.

(2) Castetter, E. F.; Opler, M. The Ethnobiology of the Chiricahua and Mescalero Apache A. In *The Use of Plants for Foods, Beverages, and Narcotics*, Studies in the American Southwest, Biological Series; The University of New Mexico Bulletin: Albuquerque, New Mexico, 1936; Vol. *III*.

(3) Martinez, M. *Las Plantas Medicinales de Mexico*, 5th ed.; Ediciones, Botas: Mexico City, 1969; pp 68−69.

(4) de Vivar, R. A.; Guerrero, C.; Wittgreen, G. Terpenoids from *Parthenium incanum*. *Rev. Latinoam. Quim.* **1970**, *1*, 39−43.

(5) de Vivar, R. A.; Matsubara, C. X-ray crystallographic studies of incanilin and argentatin B. *Rev. Latinoam. Quim.* **1986**, *17*, 7−9.

(6) Martínez-Vázquez, M.; Martínez, R.; Perez, G. E.; Diaz, M.; Sanchez, M. H. Antimicrobial properties of argentatine A, isolated from *Parthenium argentatum*. *Fitoterapia* **1994**, *65*, 371−372.

(7) Flores-Rosete, G.; Martínez-Vázquez, M. Anti-inflammatory and cytotoxic cycloartanes from guayule (*Parthenium argentatum*). *Nat. Prod. Commun.* **2008**, *3*, 413−422.

(8) Parra-Delgado, H.; Garcia-Pillado, F.; Sordo, M.; Ramirez-Apan, T.; Martínez-Vázquez, M.; Ostrosky-Wegman, P. Evaluation of the cytotoxicity, cytostaticity and genotoxicity of argentatins A and B from *Parthenium argentatum* (Gray). *Life Sci.* **2005**, *77*, 2855−2865.

(9) Romero-Benavides, J. C.; Bailon-Moscoso, N.; Parra-Delgado, H.; Ramirez, M. I.; Villacis, J.; Cabrera, H.; Gonzalez-Arevalo, G.; Cuevea, R.; Zentella-Dehesa, A.; Ratovitski, E. A.; Martínez-Vázquez, M. Argentatin B derivatives induce cell cycle arrest and DNA damage in human colon cancer cells through p73/p53 regulation. *Med. Chem. Res.* **2018**, *27*, 834−843.

(10) Duran, P.; Loya-López, S.; Ran, D.; Tang, C.; Calderon, A.; Gomez, K.; Stratton, H.; Xu, Y.-m.; Wijeratne, E. M. K.; Perez-Miller, S.; Shan, Z.; Cai, S.; Gabrielsen, A.; Dorame, A.; Masterson, K.; Alsbiei, O.; Madura, C.; Luo, G.; Moutal, A.; Streicher, J.; Gunatilaka, A. A. L.; Khanna, R. The natural product argentatin C from the medicinal plant *Parthenium incanum* attenuates postoperative pain via inhibition of voltage-gated sodium and T-type voltage-gated calcium channels. *Br. J. Pharmacol.* **2023**, *180*, 1267−1285.

(11) Institute of Medicine Report from the Committee on Advancing Pain Research, Care, and Education. *Relieving Pain in America: A Blueprint for Transforming Prevention, Care, Education and Research*; The National Academies Press: Washington DC, 2011.

(12) Quirion, B.; Bergeron, F.; Blais, V.; Gendron, L. The delta-opioid receptor; a target for the treatment of pain. *Front. Mol. Neurosci.* **2020**, *13*, 52.

(13) Desborough, M. J. R.; Keeling, D. M. The aspirin story—from willow to wonder drug. *Br. J. Haematol.* **2017**, *177*, 674−683.

(14) Zou, S.; Kumar, U. Cannabinoid receptors and the endocannabinoid system: signaling and function in the central nervous system. *Int. J. Mol. Sci.* **2018**, *19*, 833.

(15) Chung, M.-K.; Campbell, J. N. Use of capsaicin to treat pain: mechanistic and therapeutic considerations. *Pharmaceuticals* **2016**, *9*, 66.

(16) Brown, D. C. Resiniferatoxin: the evolution of the "molecular scalpel" for chronic pain relief. *Pharmaceuticals* **2016**, *9*, 47.

(17) Chin, K. Y.; Mark-Lee, W. F. A review on the antinociceptive effects of *Mitragyna speciosa* and its derivatives on animal models. *Curr. Drug Targets* **2018**, *19*, 1359−1365.

(18) Zjawiony, J. K.; Machado, A. S.; Menegatti, R.; Ghedini, P. C.; Costa, E. A.; Pedrino, G. R.; Lukas, S. E.; Franco, O. L.; Silva, O. N.; Fajemiroye, J. O. Cutting-edge search for safer opioid pain relief: retrospective review of salvinorin A and its analogs. *Front. Psychiatry* **2019**, *10*, 157.

(19) Mendes, G. L.; Santos, A. R. S.; Malheiros, A.; Filho, V. C.; Yunes, R. A.; Calixto, J. B. Assessment of mechanisms involved in antinociception caused by sesquiterpene polygodial. *J. Pharmacol. Exp. Ther.* **2000**, *292*, 164−172.

(20) Xu, Y.; Sun, J.; Li, W.; Zhang, S.; Yang, L.; Teng, Y.; Lv, K.; Liu, Y.; Su, Y.; Zhang, J.; Zhao, M. Analgesic effect of the main components of *Corydalis yanhusuo* (yanhusuo in Chinese) is caused by inhibition of voltage gated sodium channels. *J. Ethnopharmacol.* **2021**, *280*, No. 114457.

(21) Dowell, D.; Haegerich, T. M.; Chou, R. CDC Guideline for prescribing opioids for chronic pain—United States, 2016. *J. Am. Med. Assoc.* **2016**, *315*, 1624−1645.
(22) Woolf, C. J.; Hashmi, M. Use and abuse of opioid analgesics: potential methods to prevent and deter non-medical consumption of prescription opioids. *Curr. Opin. Investig. Drugs* **2004**, *5*, 61−66.
(23) Benyamin, R.; Trescot, A. M.; Datta, S.; Buenaventura, R.; Adlaka, R.; Sehgal, N.; Glaser, S. E.; Vallejo, R. Opioid complications and side effects. *Pain Physician* **2008**, *2*, S105−S120.
(24) Raja, S. N.; Carr, D. B.; Cohen, M.; Finnerup, N. B.; Flor, H.; Gibson, S.; Keefe, F. J.; Mogil, J. S.; Ringkamp, M.; Sluka, K. A.; Song, X. J.; Stevens, B.; Sullivan, M. D.; Tutelman, P. R.; Ushida, T.; Vader, K. The revised international association for the study of pain definition of pain: concepts, challenges, and compromises. *Pain* **2020**, *161*, 1976−1982.
(25) Körner, J.; Lampert, A. Functional subgroups of rat and human sensory neurons: a systematic review of electrophysiological properties. *Pflugers Arch.* **2022**, *474*, 367−385.
(26) Bennett, D. L.; Clark, A. J.; Huang, J.; Waxman, S. G.; Dib-Hajj, S. D. The Role of Voltage-Gated Sodium Channels in Pain Signaling. *Physiol. Rev.* **2019**, *99*, 1079−1151.
(27) Cai, S.; Gomez, K.; Moutal, A.; Khanna, R. Targeting T-type/CaV3. 2 channels for chronic pain. *Transl. Res.* **2021**, *234*, 20−30.
(28) Woolf, C. J. American College of Physicians; American Physiological Society. Pain: moving from symptom control toward mechanism-specific pharmacologic management. *Ann. Intern. Med.* **2004**, *140*, 441−451.
(29) Todorovic, S. M.; Jevtovic-Todorovic, V. Neuropathic pain: role for presynaptic T-type channels in nociceptive signaling. *Pflugers Arch.* **2013**, *465*, 921−927.
(30) Cheng, X.; Choi, J. S.; Waxman, S. G.; Dib-Hajj, S. D. Mini-review—sodium channels and beyond in peripheral nerve disease: Modulation by cytokines and their effector protein kinases. *Neurosci. Lett.* **2021**, *741*, No. 135446.
(31) Berta, T.; Qadri, Y.; Tan, P. H.; Ji, R. R. Targeting dorsal root ganglia and primary sensory neurons for the treatment of chronic pain. *Expert Opin. Ther. Targets* **2017**, *21*, 695−703.
(32) Bellampalli, S. S.; Ji, Y.; Moutal, A.; Cai, S.; Wijeratne, E. M. K.; Gandini, M. A.; Yu, J.; Chefdeville, A.; Dorame, A.; Chew, L. A.; Madura, C. L.; Luo, S.; Molnar, G.; Khanna, M.; Streicher, J. M.; Zamponi, G. W.; Gunatilaka, A. A. L.; Khanna, R. Betulinic acid, derived from the desert lavender *Hyptis emoryi*, attenuates paclitaxel-, HIV-, and nerve injury-associated peripheral sensory neuropathy via block of N- and T-type calcium channels. *Pain* **2019**, *160*, 117−135.
(33) Shan, Z.; Cai, S.; Yu, J.; Zhang, Z.; Vallecillo, T. G. M.; Serafini, M. J.; Thomas, A. M.; Pham, N. Y. N.; Bellampalli, S. S.; Moutal, A.; Zhou, Y.; Xu, G. B.; Xu, Y. M.; Luo, S.; Patek, M.; Streicher, J. M.; Gunatilaka, A. A. L.; Khanna, R. Reversal of peripheral neuropathic pain by the small-molecule natural product physalin F via block of CaV2.3 (R-Type) and CaV2.2 (N-Type) voltage-gated calcium channels. *ACS Chem. Neurosci.* **2019**, *10*, 2939−2955.
(34) Cai, S.; Bellampalli, S. S.; Yu, J.; Li, W.; Ji, Y.; Wijeratne, E. M. K.; Dorame, A.; Luo, S.; Shan, Z.; Khanna, M.; Moutal, A.; Streicher, J. M.; Gunatilaka, A. A. L.; Khanna, R. (−)-Hardwickiic acid and hautriwaic acid induce antinociception via blockade of tetrodotoxin-sensitive voltage-dependent sodium channels. *ACS Chem. Neurosci.* **2019**, *10*, 1716−1728.
(35) Xu, Y.-M.; Madasu, C.; Liu, M. X.; Wijeratne, E. M. K.; Dierig, D.; White, B.; Molnár, I.; Gunatilaka, A. A. L. Cycloartane and lanostane type triterpenoids from the resin of *Parthenium argentatum* AZ-2, a byproduct of guayule rubber production. *ACS Omega* **2021**, *6*, 15486−15498.
(36) (a) Rodriguez-Hahn, L.; Romo de Vivar, A.; Ortega, A.; Aguilar, M.; Romo, J. Determinación de las estructures de las argentatinas A, B y C del guayule. *Rev. Latinoam. Quim.* **1970**, *1*, 24−38. (b) de Vivar, A. R.; Martínez-Vázquez, M.; Matsubara, C.; Perez-Sanchez, G.; Joseph-Nathan, P. Triterpenes in *Parthenium argentatum*, structures of argentatins C and D. *Phytochemistry* **1990**, *29*, 915−918.
(37) Hernández-Ortega, S.; Delgado, H. P.; Martinez, M. Incaline (isoargentatin A) from *Parthenium argentatum*. *Acta Crystallogr., Sect. E: Struct. Rep. Online* **2005**, *61*, 1921−1923.
(38) Romero, J. C.; Martínez-Vázquez, A.; Herrera, M. P.; Martinez-Mayorga, K.; Parra-Delgado, H.; Pérez-Flores, F. J.; Martínez-Vázquez, M. Synthesis, anti-inflammatory activity and modeling studies of cycloartane-type terpenes derivatives isolated from *Parthenium argentatum*. *Bioorg. Med. Chem.* **2014**, *22*, 6893−6898.
(39) Escobedo-Martínez, C.; Lozada, M. C.; Hernández-Ortega, S.; Villarreal, M. L.; Gnecco, D.; Enríquez, R. G.; Reynolds, W. ^{1}H and ^{13}C NMR characterization of new cycloartane triterpenes from *Mangifera indica*. *Magn. Reson. Chem.* **2012**, *50*, 52−57.
(40) (a) Sharma, M. C.; Ohira, T.; Yatagai, M. Sericeol, a cycloartane triterpene from *Neolitsea sericea*. *Phytochemistry* **1993**, *33*, 721−722. (b) Inada, A.; Murayta, H.; Inatomi, Y.; Nakanishi, T.; Darnaedi, D. Cycloartane triterpenes from the leaves of *Aglaia harmsiana*. *J. Nat. Prod.* **1995**, *58*, 1143−1146.
(41) Karabey, F.; Khan, I. A.; Bedir, E. Cycloartane-type glycosides from *Astragalus schottianus*. *Phytochem. Lett.* **2012**, *5*, 320−324.
(42) (a) Kusumi, T.; Ohtani, L.; Inouye, Y.; Kakisawa, H. Absolute configurations of cytotoxic marine cembranolides; consideration of Mosher's method. *Tetrahedron Lett.* **1988**, *29*, 4731−4734. (b) Ohtani, I.; Kusumi, T.; Kashman, Y.; Kakisawa, H. High-field FT NMR application of Mosher's method. The absolute configurations of marine terpenoids. *J. Am. Chem. Soc.* **1991**, *113*, 4092−4096. (c) Su, B. N.; Park, E. J.; Mbwambo, Z. H.; Santarsiero, B. D.; Mesecar, A. D.; Fong, H. H. S.; Pezzuto, J. M.; Kinghorn, A. D. New chemical constituents of *Euphorbia quinquecostata* and absolute configuration assignment by a convenient Mosher ester procedure carried out in NMR tubes. *J. Nat. Prod.* **2002**, *65*, 1278−1282.
(43) Hille, B. Local anesthetics: hydrophilic and hydrophobic pathways for the drug-receptor reaction. *J. Gen. Physiol.* **1977**, *69*, 497−515.
(44) Jiang, D.; Shi, H.; Tonggu, L.; El-Din, T. M. G.; Lenaeus, M. J.; Zhao, Y.; Yoshioka, C.; Zheng, N.; Catterall, W. A. Structure of cardiac sodium channel. *Cell* **2020**, *180*, 122−134.e10.
(45) Li, X.; Xu, F.; Xu, H.; Zhang, S.; Gao, Y.; Zhang, H.; Dong, Y.; Zheng, Y.; Yang, B.; Sun, J.; Zhang, X. C.; Zhao, Y.; Jiang, D. Structural basis for modulation of human Nav1.3 by clinical drug and selective anatagonist. *Nat. Commun.* **2022**, *13*, No. 1286.
(46) Zhang, J.; Shi, Y.; Huang, Z.; Li, Y.; Yang, B.; Gong, J.; Jiang, D. Structural basis for Nav1.7 inhibition by pore blockers. *Nat. Struct. Mol. Biol.* **2022**, *29*, 1208−1216.
(47) Huang, X.; Jin, X.; Huang, G.; Huang, J.; Wu, T.; Li, Z.; Chen, J.; Kong, F.; Pan, X.; Yan, N. Structural basis for high-voltage activation and subtype-specific inhibition of human Nav1.8. *Proc. Natl. Acad. Sci. U.S.A.* **2022**, *119*, No. e2208211119.
(48) Zhao, Y.; Huang, G.; Wu, Q.; Wu, K.; Li, R.; Lei, J.; Pan, X.; Yan, N. Cryo-EM structures of apo and antagonist-bound human Cav3.1. *Nature* **2019**, *576*, 492−497.
(49) Yao, X.; Gao, S.; Yan, N. Structural basis for pore blockade of human voltage-gated calcium channel Cav1.3 by motion sickness drug cinnarizine. *Cell Res.* **2022**, *32*, 946−948.
(50) Dong, Y.; Gao, Y.; Xu, S.; Wang, Y.; Yu, Z.; Li, Y.; Li, B.; Yuan, T.; Yang, B.; Zhang, X. C.; Jiang, D.; Huang, Z.; Zhao, Y. Closed-state inactivation and pore-blocker modulation mechanisms of human Cav2.2. *Cell Rep.* **2021**, *37*, No. 109931.
(51) He, L.; Yu, Z.; Geng, Z.; Huang, Z.; Zhang, C.; Dong, Y.; Gao, Y.; Wang, Y.; Chen, Q.; Sun, L.; Ma, X.; Huang, B.; Wang, X.; Zhao, Y. Structure, gating, and pharmacology of human Cav3.3 channel. *Nat. Commun.* **2022**, *13*, No. 2084.
(52) Xie, M. X.; Yang, J.; Pang, R. P.; Zeng, W. A.; Ouyang, H. D.; Liu, Y. Q.; Liu, X. G. Bulleyaconitine A attenuates hyperexcitability of dorsal root ganglion neurons induced by spared nerve injury: The role of preferably blocking Nav1.7 and Nav1.3 channels. *Mol. Pain* **2018**, *14*, No. 1744806918778491.
(53) Bregman, H.; Berry, L.; Buchanan, J. L.; Chen, A.; Du, B.; Feric, E.; Hierl, M.; Huang, L.; Immke, D.; Janosky, B.; Johnson, D.; Li, X.; Ligutti, J.; Liu, D.; Malmberg, A.; Matson, D.; McDermott, J.; Miu, P.;

https://doi.org/10.1021/acsomega.3c02302
ACS Omega 2023, 8, 20085−20095

Nguyen, H. N.; Patel, V. F.; Waldon, D.; Wilenkin, B.; Zheng, X. M.; Zou, A.; McDonough, S. I.; DiMauro, E. F. Identification of a potent, state-dependent inhibitor of Nav1.7 with oral efficacy in the formalin model of persistent pain. *J. Med. Chem.* **2011**, *54*, 4427−4445.
(54) Jarvis, M. F.; Honore, P.; Shieh, C. C.; Chapman, M.; Joshi, S.; Zhang, X. F.; Kort, M.; Carroll, W.; Marron, B.; Atkinson, R.; Thomas, J.; Liu, D.; Krambis, M.; Liu, Y.; McGaraughty, S.; Chu, K.; Roeloffs, R.; Zhong, C.; Mikusa, J. P.; Hernandez, G.; Gauvin, D.; Wade, C.; Zhu, C.; Pai, M.; Scanio, M.; Shi, L.; Drizin, I.; Gregg, R.; Matulenko, M.; Hakeem, A.; Gross, M.; Johnson, M.; Marsh, K.; Wagoner, P. K.; Sullivan, J. P.; Faltynek, C. R.; Krafte, D. S. A-803467, a potent and selective Nav1.8 sodium channel blocker, attenuates neuropathic and inflammatory pain in the rat. *Proc. Natl. Acad. Sci. U.S.A.* **2007**, *104*, 8520−8525.
(55) Lee, M. Z944: a first in class T-type calcium channel modulator for the treatment of pain. *J. Peripher. Nerv. Syst.* **2014**, *19*, S11−S12.
(56) Wall, M. J.; Subasinghe, N. L.; Winters, M. P.; Lubin, M. L.; Finley, M. F. A.; Qin, N.; Brandt, M. R.; Neeper, M. P.; Schneider, C. R.; Colburn, R. W.; Flores, C. M.; Sui, Z. Discovery and optimization of a novel series of pyrazolyltetrahydropyran N-type calcium channel (Ca_v 2.2) blockers for the treatment of pain. *Bioorg. Med. Chem. Lett.* **2018**, *28*, 3780−3783.
(57) Robetta Protein Structure Prediction Service, 2022. https://robetta.bakerlab.org.
(58) Shen, H.; Liu, D.; Wu, K.; Lei, J.; Yan, N. Structures of human Nav1.7 channel in complex with auxiliary sub-units and animal toxins. *Science* **2019**, *363*, 1303−1308.
(59) *Schrödinger Release 2020-4*; Schrödinger, LLC: New York, NY, 2020.
(60) Madhavi Sastry, G.; Adzhigirey, M.; Day, T.; Annabhimoju, R.; Sherman, W. Protein and ligand preparation: parameters, protocols, and influence on virtual screening enrichments. *J. Comput.-Aided Mol. Des.* **2013**, *27*, 221−234.
(61) Friesner, R. A.; Banks, J. L.; Murphy, R. B.; Halgren, T. A.; Klicic, J. J.; Mainz, D. T.; Repasky, M. P.; Knoll, E. H.; Shelley, M.; Perry, J. K.; Shaw, D. E.; Francis, P.; Shenkin, P. S. Glide: a new approach for rapid, accurate docking and scoring. 1. Method and assessment of docking accuracy. *J. Med. Chem.* **2004**, *47*, 1739−1749.
(62) *The PyMOL Molecular Graphics System*, version 2.0; Schrödinger, LLC, 2022.

https://doi.org/10.1021/acsomega.3c02302
ACS Omega 2023, 8, 20085−20095